Multi-orbital effects in optical properties of vanadium sesquioxide

2009 J. Phys.: Condens. Matter 21 064209

(http://iopscience.iop.org/0953-8984/21/6/064209)

J. Phys.: Condens. Matter **21** (2009) 064209 (5pp) doi:10.1088/0953-8984/21/6/064209

Multi-orbital effects in optical properties of vanadium sesquioxide

Jan M Tomczak[1,2] **and Silke Biermann**[2,3]

[1] Research Institute for Computational Sciences, AIST, Tsukuba 305-8568, Japan
[2] Japan Science and Technology Agency, CREST, Japan
[3] Centre de Physique Théorique, Ecole Polytechnique, 91128 Palaiseau Cedex, France

E-mail: jan.tomczak@polytechnique.edu

Received 28 June 2008, in final form 1 September 2008
Published 20 January 2009
Online at stacks.iop.org/JPhysCM/21/064209

Abstract
Vanadium sesquioxide, V_2O_3, boasts a rich phase diagram whose description necessitates accounting for many-body Coulomb correlations. The spectral properties of this compound have been successfully addressed within dynamical mean field theory to the extent that results of recent angle-resolved photoemission experiments have been correctly predicted. While photoemission spectroscopy probes the occupied part of the one-particle spectrum, optical experiments measure transitions into empty states and thus provide complementary information. In this work, we focus on the optical properties of V_2O_3 in its paramagnetic phases by employing our recently developed 'generalized Peierls approach'. We obtain results in overall satisfactory agreement with experiments. Further, we rationalize that the experimentally observed temperature dependence stems from the different coherence scales of the charge carriers involved.

(Some figures in this article are in colour only in the electronic version)

1. Introduction

Vanadium sesquioxide, V_2O_3, has been the subject of extensive theoretical and experimental studies for more than three decades. It is considered as *the* prototype compound, that undergoes a Mott–Hubbard transition [1, 2] in its purest form. Indeed, the high-temperature ($T > T_{\text{Néel}}$) metal–insulator transition upon chemical substitution, $(V_{1-x}Cr_x)_2O_3$, is isostructural and no magnetic order is acquired. Early theoretical approaches resorted to the Hubbard model to explain the electronic properties of V_2O_3. However, over the years, experiments indicated that the physics of this material is more involved and a realistic multi-orbital setup is needed for the complexity of the correlation effects taking place (for reviews see e.g. [1–3]).

The field of correlated materials gained major momentum from the development of dynamical mean field theory (DMFT) [4]. In combination with standard density functional based methods like the local density approximation (LDA) the calculation of spectral properties of materials with strong electronic Coulomb interactions became possible. Over the past years, LDA + DMFT increased our understanding of materials such as transition metals, their oxides or sulfides, as well as f-electron compounds [5]. Several works highlighted the applicability of the technique to V_2O_3 [6–11]. In our previous work [11], we find that the metal–insulator transition is not due to the Brinkman–Rice mechanism [12] in its single-band form, but results from the impact of Coulomb correlations on the crystal-field splitting. Owing to its octahedral oxygen surroundings, the vanadium 3d orbitals split into two e_g^σ and three lower lying t_{2g} orbitals. The two manifolds of bands are isolated in energy, both from each other and from other orbitals. The trigonal part of the crystal field further splits the t_{2g} into an a_{1g} and two lower lying degenerate e_g^π orbitals. The local Coulomb correlations result in an increased a_{1g}–e_g^π splitting with respect to the LDA, causing a charge transfer that pushes a_{1g} spectral weight above the Fermi level. By computing momentum-resolved spectral functions [13, 14, 11], we made explicit predictions for angle-resolved photoemission experiments. Recent measurements on $(V_{1-x}Cr_x)_2O_3$ ($x = 0.011$) [15] nicely agree with the theoretical spectra, further validating our current understanding of this compound.

2. Optical properties—prelude

Optical spectroscopy is an experimental probe complementary to photoemission which is commonly analyzed in terms of the

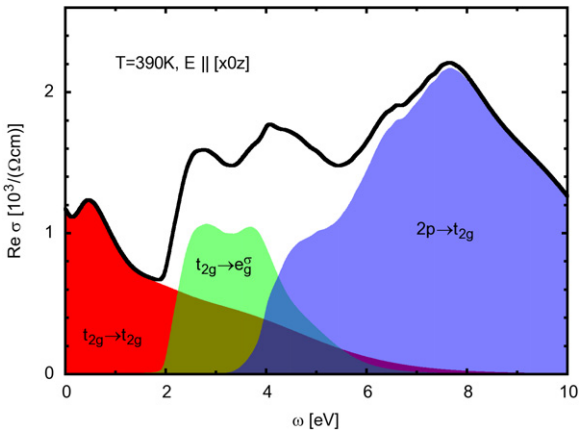

Figure 1. Theoretical optical conductivity of V_2O_3 at $T \approx 390$ K for a light polarization $E \parallel [x\ 0\ z] = [0.13, 0.0, 0.041]$. Contributions from different energy sectors (see appendix A.2): $t_{2g} \rightarrow t_{2g}$, $t_{2g} \rightarrow e_g^\sigma$, O2p $\rightarrow t_{2g}$.

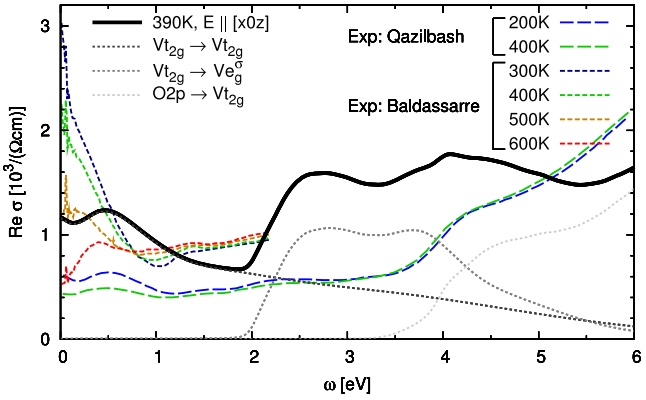

Figure 2. Theoretical and experimental conductivity of V_2O_3. Theory (same polarization as in figure 1): total (bold), orbital contributions (dotted). Experiments: polycrystalline film, ($T = 200$, 400 K) Qazilbash *et al* [23] (long dashed), single crystal ($T = 300$–600 K) Baldassarre *et al* [24] (short dashed).

optical conductivity [16]

$$\mathrm{Re}\,\sigma^{\alpha\beta}(\omega) = \frac{2\pi e^2\hbar}{V}\sum_{\mathbf{k}}\int \mathrm{d}\omega'\,\frac{f(\omega') - f(\omega'+\omega)}{\omega} \times \mathrm{tr}\{A_{\mathbf{k}}(\omega'+\omega)v_{\mathbf{k},\alpha}A_{\mathbf{k}}(\omega')v_{\mathbf{k},\beta}\} \quad (1)$$

that is given by a convolution of spectral functions $A_{\mathbf{k}}(\omega)$.[4] The transitions are weighted by dipole matrix elements, called Fermi velocities, $v_{\mathbf{k},\alpha}$, and the Fermi functions $f(\omega)$ select the range of occupied and empty states, respectively. V is the unit-cell volume, α, β denote Cartesian coordinates, and $\Re\sigma^{\alpha\beta}$ is the response in the α-direction for light polarization along β. Both spectral functions and velocities are matrices in the basis of localized orbitals, which we index by $L = (n, l, m, \gamma)$, with the usual quantum numbers (n, l, m), while γ labels the individual atoms in the unit cell. While the computation of the Fermi velocities is straightforward, e.g. in a plane-wave basis, their evaluation becomes tedious when using localized orbitals as required by many-body approaches such as LDA + DMFT. To this end, we employ the recently generalized Peierls approach [3, 18, 19], which we briefly summarize in appendix A.1.

In their pioneering work, Rozenberg *et al* [20] analyzed the optical conductivity of V_2O_3 from the model perspective. It was concluded that the phenomenology of the temperature dependence in the conductivity can be understood by appealing to the physics of the one-band Hubbard model. In the current work, we will substantiate and extend these observations, based on a realistic multi-band setup.

3. Optical properties—results

Our calculation of the optical conductivity is based on the previous LDA + DMFT electronic structure computation of [11], which used a one-particle Hamiltonian that was downfolded [21, 22] to the vanadium t_{2g} orbitals. Since optical experiments normally probe a much wider frequency range, we employ an upfolding scheme that includes higher energy states on the LDA level. Details are summarized in appendix A.2.

Figure 1 shows our theoretical optical conductivity for V_2O_3 at $T = 390$ K for the indicated light polarization. While in the Kohn–Sham spectrum, the t_{2g} and e_g^σ bands are well separated, the correlations—accounted for by LDA + DMFT for the t_{2g} orbitals only [11]—result in an intra-t_{2g} conductivity that has weight up to energies well beyond the onset of transitions into the e_g^σ at about 2 eV. Contributions stemming from transitions from the occupied oxygen 2p orbitals into the t_{2g} occur from around 3.5 eV onwards.

Before turning to a more detailed analysis of the different orbital contributions we compare our results to experimental data (see figure 2). First, we notice the discrepancies *between the experiments*: recent measurements on single crystals [24] agree well with previous single crystal experiments [20], but they are at variance with measurements using a polycrystalline film [23]. While the use of polycrystalline samples, especially in a metal, might be an issue, so is the fact that both single crystal experiments were performed up to energies of only a few eV although the extraction of the conductivity involves a Kramers–Kronig transform. The low energy shape of the theoretical conductivity resembles the polycrystalline conductivity, but the absolute values differ. As to the single crystal one, we note that the order of magnitude compares favorably, while the shape tends to be comparable with the high temperature curves only.

At high energies, we see that both the onset and the shape of oxygen 2p derived contributions agree with experiment. The upfolding scheme that uses the 2p bands from LDA is thus a good approximation. This seems not to be true for transitions into e_g^σ orbitals: compared with experiment [23], we realize that the spectral weight is too sharply defined and no identification of particular structures is possible. This calls

[4] In the case of a single orbital, vertex-corrections vanish in the limit of infinite lattice coordination [17]. Therefore the response can be expressed in terms of spectral functions. In the general multi-orbital case this is an approximation.

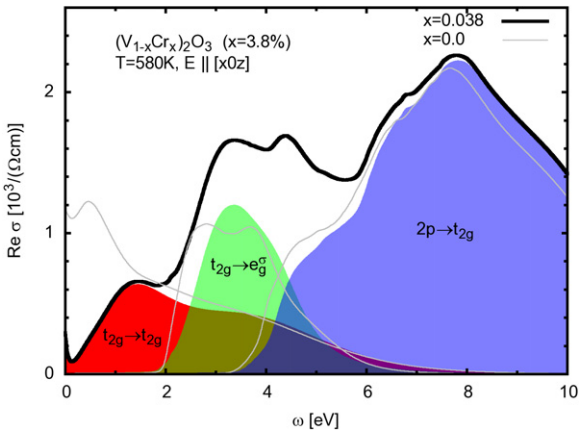

Figure 3. Theoretical optical conductivity of $(V_{1-x}Cr_x)_2O_3$, $x = 3.8\%$ at $T = 580$ K for a light polarization $E \parallel [x\ 0\ z] = [0.13, 0.0, 0.0415]$. Contributions from different energy sectors: $t_{2g} \rightarrow t_{2g}$, $t_{2g} \rightarrow e_g^{\sigma}$, O2p $\rightarrow t_{2g}$. Gray lines show the results for pure V_2O_3 (figure 1) for comparison.

for an LDA + DMFT calculation that includes all vanadium 3d orbitals.

We now turn to a detailed analysis of orbital effects in the optical conductivity. This is a topic that has not been dealt with so far, since previous work neglected inter-band transitions altogether [24].

At low energy only a small Drude-like tail appears. This can be understood from the underlying electronic structure. Indeed, the metallic character of V_2O_3 is mainly a result of a_{1g} charge carriers that have spectral weight at the Fermi level only in a very limited region of the Brillouin zone (BZ), as can be seen in figure 4 of [11].

As can also be inferred from that work, the local spectral functions of a_{1g} and e_g^{π} character display a pseudo-gap-like behavior, and peak at finite energies rather than at the Fermi level, accounting for the feature seen at 0.5 eV in the conductivity. The latter originates from two types of transitions[5]: at energies lower than 0.6 eV the spectral weight is mainly due to transitions from a_{1g} into low lying e_g^{π} orbitals, that are restricted to a small region in the BZ, whereas at slightly higher energies, 0.6 eV and above, the majority of contributions derive from e_g^{π} to e_g^{π} transitions, which are possible in a wide region of the BZ, yet are less prominent at the Γ-point.

At this point we again use our knowledge about the electronic structure of the compound: Poteryaev *et al* [11] established an important orbital dependence of the quasi-particle coherence scale. Indeed, down to 390 K, e_g^{π} excitations are far from being coherent: the imaginary part of the e_g^{π} self-energy reaches −0.45 eV at the Fermi level, while a_{1g} excitations have reached their coherence regime in our calculation [11, 3]. Thus ($e_g{}^{\pi}$) a_{1g} carriers are (not) particularly sensitive to changes in temperature. As discussed above, the low energy (<0.6 eV) optical response is determined by a_{1g}–e_g^{π} transitions, while above 0.6 eV e_g^{π}–e_g^{π} transitions become dominant. Given these two facts, one can—even without explicit calculations—make some predictions about the behavior of the optical response when the temperature is raised: upon heating, the purely e_g^{π}-derived contributions will not change as much as will those that involve the a_{1g} orbitals, so that the low energy response will be more sensitive than the weight beyond 0.6 eV. In particular, a broadening (and thus reduction in height) is expected for the very low energy part. This gives a natural explanation for the dip behavior that is observed in the experiments when the temperature is raised above ∼450 K (see figure 1 in [24] or our figure 2)[6]. Explicit calculations as a function of temperature (including inter-band transitions) would be desirable to confirm the picture emerging from our results. This challenging project is left for future work.

In figure 3 we show theoretical results for the insulator $(V_{1-x}Cr_x)_2O_3$ ($x = 3.8\%$). As discussed previously [11], we have low but finite spectral weight at the Fermi level, which results in some optical weight at low frequency. Unfortunately, no experimental data are available for this composition. Compared with pure V_2O_3, we note the suppression of low energy spectral weight and the clear distinction of transitions into the t_{2g} upper Hubbard bands at ∼4 eV.

4. Conclusions

In conclusion, we have presented calculations of the optical conductivity of V_2O_3 in its paramagnetic phases using the generalized Peierls approach. We obtain good agreement with experiment and propose an explanation for the experimentally shown temperature dependence of the response as a signature of the orbital-selective coherence of the system. Our upfolding scheme to include higher energy orbitals captures well the transitions involving oxygen states, but reveals the necessity of including all 3d orbitals in a LDA + DMFT electronic structure calculation for this compound.

Acknowledgments

We thank M M Qazilbash, M Marsi and A I Lichtenstein for discussions on optical and photoemission spectroscopy. Moreover, we thank our co-authors of [11], and in particular A I Poteryaev, for the collaboration on the electronic structure of V_2O_3, that was our starting point. JMT kindly acknowledges support by the Ecole Polytechnique, where this work began. This work was supported by the French ANR under project CORRELMAT, and by Idris, Orsay, under project no. 081393.

[5] The following is inferred from 'momentum-resolved optics', i.e. from distinguishing contributions of different points in the Brillouin zone (not shown, see [3]).

[6] Reference [24] has invoked the change of the lattice constants upon heating in order to explain this dip. It is clear that the mechanism based on the orbital-selective coherence that emerges from our work could not have been observed in the calculation of Baldassarre *et al* since, there, inter-band transitions were neglected (see their footnote 26 and our discussion in appendix A.1).

Appendix. Details of the formalism

A.1. Generalized Peierls substitution approach to Fermi velocities

The Fermi velocities in (1) are given by elements of the momentum operator $\mathcal{P}$:

$$v^{L'L}_{\mathbf{k},\alpha} = \frac{1}{m}\langle \mathbf{k}L'|\mathcal{P}_\alpha|\mathbf{k}L\rangle \tag{A.1}$$

$L = (n, l, m, \gamma)$ and γ labels atoms in the unit-cell. Equation (A.1) is easily calculated in plane waves, while using a localized Wannier-like basis $\chi_{\mathbf{R}L}(\mathbf{r}) = \langle \mathbf{r}|\mathbf{R}L\rangle = \sum_{\mathbf{k}} \mathrm{e}^{-\mathrm{i}\mathbf{k}\mathbf{R}}\langle \mathbf{r}|\mathbf{k}L\rangle$ renders the evaluation tedious. Inspired by the Peierls substitution approach [16] for lattice models, we can separate the above into [3, 18, 19]:

$$v^{L'L}_{\mathbf{k},\alpha} = \frac{1}{\hbar}(\partial_{k_\alpha}\mathbf{H}^{L'L}_{\mathbf{k}} - \mathrm{i}(\rho^\alpha_{L'} - \rho^\alpha_L)\mathbf{H}^{L'L}_{\mathbf{k}}) + \mathcal{F}_{\mathbf{H}}[\{\chi_{\mathbf{R}L}\}]. \tag{A.2}$$

The terms in brackets are the Fermi velocity in the Peierls approximation, which is here generalized to a multi-atomic unit-cell: ρ^α_L is the α-component of the position of atom γ within the unit-cell. This velocity is easy to evaluate since it involves only elements of the Hamiltonian. It is crucial that $\mathcal{F}_{\mathbf{H}}[\{\chi_{\mathbf{R}L}\}]$ reduces to intra-atomic contributions in the limit of strongly localized orbitals $\chi_{\mathbf{R}L}$ [3], which makes the generalized Peierls velocity a good approximation for 3d and 4f systems for example.

Finally, we ask if the computation of the Fermi velocities is really necessary in practice, or if one could also resort to a simpler approximation consisting of simply omitting the Fermi velocities. Due to its simplicity, this approximation is in fact relatively popular for obtaining qualitative trends of optical properties in correlated systems [24, 25]. Since the conductivity is then a simple convolution of spectral functions, inter-band transitions ($L \neq L'$) are neglected and intra-band transitions not properly weighted. As an illustration, we show in figure A.1 a comparison of the optical conductivity calculated within the generalized Peierls formalism compared to the one computed from the simple convolution of spectral functions[7]: besides the obvious discrepancy in absolute value, omitting the Fermi velocities results in a noticeable change in shape too. This is owing to the momentum dependence of the matrix elements that favors certain regions in the Brillouin zone while attenuating others.

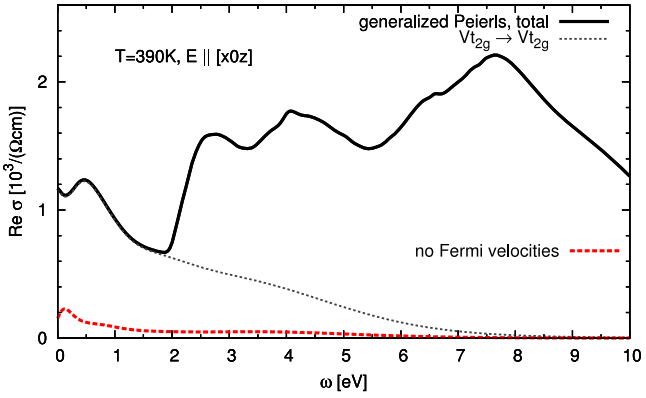

Figure A.1. Generalized Peierls conductivity versus the 'no velocity approximation'.

A.2. Upfolding scheme for higher energy transitions

Although the treatment of many-body correlations can often be cast into an effective low energy, downfolded system, the range of its validity is usually far exceeded by optical measurements. Thus it is desirable to allow for optical transitions into higher energy orbitals. Also, the computation of the Fermi velocities and the downfolding procedure do not commute [16], and hence it makes a difference to which Hamiltonian the generalized Peierls approach is applied. As a matter of fact, the Wannier functions of a full Hamiltonian are more localized than those of the downfolded one, whereby the Peierls approximation becomes more accurate[8]. The key quantity for the conductivity is the orbital trace in (1). For any unitary transformation $U_{\mathbf{k}}$ holds

$$\begin{aligned}&\mathrm{tr}\{v_{\mathbf{k}}A_{\mathbf{k}}(\omega')v_{\mathbf{k}}A_{\mathbf{k}}(\omega'+\omega)\}\\ &\quad = \mathrm{tr}\{U^\dagger_{\mathbf{k}}v_{\mathbf{k}}U_{\mathbf{k}}\widetilde{A}_{\mathbf{k}}(\omega')U^\dagger_{\mathbf{k}}v_{\mathbf{k}}U_{\mathbf{k}}\widetilde{A}_{\mathbf{k}}(\omega'+\omega)\}\end{aligned} \tag{A.3}$$

where we defined $\widetilde{A}_{\mathbf{k}} = U^\dagger_{\mathbf{k}}A_{\mathbf{k}}U_{\mathbf{k}}$. In the case of a pure band-structure calculation (no self-energy), we can choose the transformation such that it performs the downfolding, i.e. the spectral functions $\widetilde{A}_{\mathbf{k}}$, acquire a block-diagonal form. We shall distinguish between the low energy ($\mathscr{L}$) and the high energy block ($\mathscr{H}$): an LDA + DMFT calculation will add local Coulomb interactions only to the former *after* the block-diagonalization, which results in a self-energy that lives in this sub-block, while high energy bands remain unchanged and the block-diagonality is retained. Clearly the downfolding procedure is not exact in the many-body framework. Indeed the matrices that block-diagonalize the true interacting system also depend on frequency, due to the dynamical nature of the self-energy. Yet, when granting the approximate validity of the downfolding, and using the $U_{\mathbf{k}}$ of the band-structure calculation, we can specify

$$\begin{aligned}\widetilde{v}_{\mathbf{k}} = \begin{pmatrix} V_1 & W \\ W^\dagger & V_2 \end{pmatrix}, \qquad \widetilde{A}_{\mathbf{k}}(\omega') = \begin{pmatrix} L & 0 \\ 0 & H \end{pmatrix},\\ \widetilde{A}_{\mathbf{k}}(\omega'+\omega) = \begin{pmatrix} \bar{L} & 0 \\ 0 & \bar{H} \end{pmatrix}\end{aligned} \tag{A.4}$$

with $\widetilde{v}_{\mathbf{k}} = U^\dagger_{\mathbf{k}}v_{\mathbf{k}}U_{\mathbf{k}}$. The many-body spectra L, $\bar{L}$ are substituted into the $\mathscr{L}$-sector, while H, $\bar{H}$ of the $\mathscr{H}$-sector stem from the initial band-structure, and (A.3) read

$$LV_1\bar{L}V_1 + LW\bar{H}W^\dagger + HV_2\bar{H}V_2 + HW^\dagger\bar{L}W. \tag{A.5}$$

For transitions within the $\mathscr{L}$-block, the velocity V_1 appears, which is the $\mathscr{L}$-block of the *transformed* velocity. It is

[7] In order to have comparable scales, we chose for the latter case $v_{\mathbf{k}} = r_0\,\mathbb{I}$, with the Bohr radius r_0.

[8] Indeed the downfolding can be viewed as a unitary transformation that block-diagonalizes the Hamiltonian (see below). The change in accuracy manifests itself in the basis dependence of the optical conductivity within the Peierls approach.

different from the element computed *after* the downfolding. With the above, we moreover include transitions from, to and within the high energy block[9]. Comparison to experiments then allows one to assess whether correlation effects substantially modify the spectrum of downfolded orbitals as well, or whether for them the initial band-structure is satisfying (see above for the V_2O_3 case).

References

[1] Mott N F 1990 *Metal–Insulator Transition* (London: Taylor and Francis)

[2] Imada M, Fujimori A and Tokura Y 1998 Metal–insulator transitions *Rev. Mod. Phys.* **70** 1039–263

[3] Tomczak J M 2007 Spectral and optical properties of correlated materials *PhD Thesis* Ecole Polytechnique, France

[4] Georges A, Kotliar G, Krauth W and Rozenberg M J 1996 Dynamical mean-field theory of strongly correlated fermion systems and the limit of infinite dimensions *Rev. Mod. Phys.* **68** 13

[5] Kotliar G and Vollhardt D 2004 Strongly correlated materials: insights from dynamical mean-field theory *Phys. Today* **57** 53

[6] Held K, Keller G, Eyert V, Vollhardt D and Anisimov V I 2001 Mott–Hubbard metal–insulator transition in paramagnetic V_2O_3: an LDA + DMFT (QMC) study *Phys. Rev. Lett.* **86** 5345–8

[7] Keller G, Held K, Eyert V, Vollhardt D and Anisimov V I 2004 Electronic structure of paramagnetic V_2O_3: strongly correlated metallic and Mott insulating phase *Phys. Rev.* B **70** 205116

[8] Laad M S, Craco L and Müller-Hartmann E 2003 Orbital switching and the first-order insulator–metal transition in paramagnetic V_2O_3 *Phys. Rev. Lett.* **91** 156402

[9] Laad M S, Craco L and Muller-Hartmann E 2006 Orbital-selective insulator–metal transition in V_2O_3 under external pressure *Phys. Rev.* B **73** 045109

[10] Anisimov V I, Kondakov D E, Kozhevnikov A V, Nekrasov I A, Pchelkina Z V, Allen J W, Mo S-K, Kim H-D, Metcalf P, Suga S, Sekiyama A, Keller G, Leonov I, Ren X and Vollhardt D 2005 Full orbital calculation scheme for materials with strongly correlated electrons *Phys. Rev.* B **71** 125119

[11] Poteryaev A I, Tomczak J M, Biermann S, Georges A, Lichtenstein A I, Rubtsov A N, Saha-Dasgupta T and Andersen O K 2007 Enhanced crystal-field splitting and orbital-selective coherence induced by strong correlations in V_2O_3 *Phys. Rev.* B **76** 085127

[12] Brinkman W F and Rice T M 1970 Application of Gutzwiller's variational method to the metal–insulator transition *Phys. Rev.* B **2** 4302–4

[13] Tomczak J M and Biermann S 2007 Effective band structure of correlated materials: the case of VO_2 *J. Phys.: Condens. Matter* **19** 365206

[14] Tomczak Jan M, Aryasetiawan F and Biermann S 2008 Effective bandstructure in the insulating phase versus strong dynamical correlations in metallic VO_2 *Phys. Rev.* B **78** 115103

[15] Rodolakis F, Mansart B, Rueff J P, Vilmercati P, Petaccia L, Goldoni A, Lupi S, Metcalf P and Marsi M 2008 Mott–Hubbard transition in Cr-doped V_2O_3 studied with low energy photoemission, private communication, unpublished

[16] Millis A J 2004 Optical conductivity and correlated electron physics *Strong Interactions in Low Dimensions* vol 25, ed L Degiorgi and D Baeriswyl (Heidelberg: Springer) p 195

[17] Khurana A 1990 Electrical conductivity in the infinite-dimensional Hubbard model *Phys. Rev. Lett.* **64** 1990

[18] Tomczak J M and Biermann S 2008 Materials design using correlated oxides: optical properties of vanadium dioxide *Phys. Rev. Lett.* submitted (Tomczak J M and Biermann S 2008 [arXiv:0807.4044])

[19] Tomczak J M and Biermann S 2008 Optical properties of correlated materials—or why intelligent windows may look dirty Ψ_k *Scientific Highlight of the Month* (88) (August) http://www.psi-k.org/newsletters/News_88/Highlight_88.pdf

[20] Rozenberg M J, Kotliar G, Kajueter H, Thomas G A, Rapkine D H, Honig J M and Metcalf P 1995 Optical conductivity in Mott–Hubbard systems *Phys. Rev. Lett.* **75** 105–8

[21] Löwdin P-O 1951 A note on the quantum-mechanical perturbation theory *J. Chem. Phys.* **19** 1396

[22] Andersen O K and Saha-Dasgupta T 2000 Muffin-tin orbitals of arbitrary order *Phys. Rev.* B **62** R16219–22

[23] Qazilbash M M, Schafgans A A, Burch K S, Yun S J, Chae B G, Kim B J, Kim H T and Basov D N 2008 Electrodynamics of the vanadium oxides VO_2 and V_2O_3 *Phys. Rev.* B **77** 115121

[24] Baldassarre L, Perucchi A, Nicoletti D, Toschi A, Sangiovanni G, Held K, Capone M, Ortolani M, Malavasi L, Marsi M, Metcalf P, Postorino P and Lupi S 2008 Quasiparticle evolution and pseudogap formation in V_2O_3: an infrared spectroscopy study *Phys. Rev.* B **77** 113107

[25] Pavarini E, Yamasaki A, Nuss J and Andersen O K 2005 How chemistry controls electron localization in $3d^1$ perovskites: a Wannier-function study *New J. Phys.* **7** 188

[9] We can thus distinguish different origins of spectral weight. Yet we cannot tell apart contributions within the $\mathscr{L}$-block. While one can suppress selected transitions by setting Fermi-velocity matrix elements to zero, contributions are in that case not additive.